



Cite this: *RSC Adv.*, 2024, 14, 39740

Controllable synthesis of Co/NC catalysts with high-density Co–N_x active sites derived from Co/Zn-ZIF for cyclopropanation†

Xin Yue, Jiangwei Li, Chunying Li, Zhixuan Wang, Yongmei Du, Daoan Sun,  * Hui Ma and Jian Lu*

Received 9th March 2024
Accepted 22nd October 2024

DOI: 10.1039/d4ra01816h

rsc.li/rsc-advances

Novel Co/NC heterogeneous catalysts were prepared by simply employing self-made Co/Zn-ZIF (zeolitic imidazolate framework) through pyrolysis. The samples were characterized by XRD, XPS, Raman, TEM and BET, and were successfully applied in a cyclopropanation reaction with a yield of 85%. Furthermore, this one-pot synthesized catalyst could be recycled several times without apparent deactivation. The content of Co–N_x active sites could be modified by adjusting the Co/Zn molar ratio of the ZIF precursor. The generation of Co–N_x could be attributed to the evaporation of Zn species, which provides rich micropores.

Introduction

The cyclopropane ring structure exhibits specific bioactivity in many medical materials and has become an important structural unit in pharmaceutical chemistry, attracting great research interest.^{1–3} Meanwhile, the highly strained energy of the three-numbered ring makes cyclopropane a valuable candidate for the synthesis of high-energy-density fuels. Various synthetic methods for cyclopropanation have been developed, such as Simmons–Smith reaction, diazo-derived cyclopropanation, free carbenes *via* α -Elimination and Kulinkovich reaction.^{4–8} Particularly, the cyclopropanation of alkenes with diazo compounds stands out as the most atom-economic strategy.⁹ However, most studies have employed homogeneous catalysts, such as Fe, Ru, Rh, Co and Cu complexes, leading to problems like difficulty in separation, low reusability and high costs.^{10–16} To tackle these challenges, developing highly active, recyclable heterogeneous catalysts using inexpensive metal is desirable.

To date, a few reports describe the use of heterogeneous catalysts for cyclopropanation, such as CuO–TiO₂/Al₂O₃, CuNPs–Al₂O₃, core–shell Cu–Fe NPs and silver/copper foil.^{17–21} Nevertheless, these catalysts, originating from complex preparation methods, display low catalytic efficiency due to lack of controllable active sites.^{22–25} The preparation of high-performance heterogeneous catalysts for cyclopropanation calls for a simple method to produce abundant active sites. Recently, a new design involving 3d transition metals and an N-

doped carbon system (M–N–C) has garnered attention in materials sciences.^{26–28} More specifically, engineering abundant active sites *via* the evaporation of Zn species during the pyrolysis of zeolitic imidazolate frameworks (ZIFs) has generated significant interest for producing more complex microstructures.^{29–34} We believe that applying this method to prepare heterogeneous catalysts could increase the number of active sites, leading to better yields in cyclopropanation.^{35,36} In this paper, we report on Co-based heterogeneous catalysts for cyclopropanation and present an *in situ* method for the controllable production of Co–N_x active sites on these Co/NC catalysts by adjusting the Co/Zn molar of Co/Zn-ZIFs.

Experimental

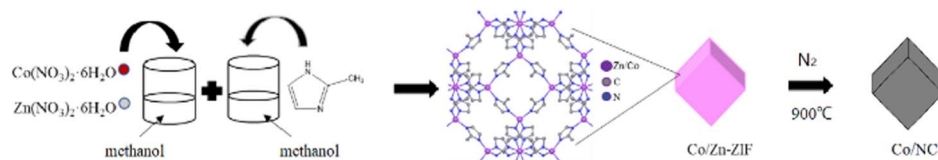
Preparation of catalysts

Co@N-doped carbon materials labeled as Co_x/NC-*T* (where *x* represents the molar ratio and *T* indicates the calcination temperature), were synthesized using a simple method, as shown in Scheme 1. Co/Zn-ZIFs were synthesized from an aqueous solution at room temperature. Typically, a total of 10 mmol mixture of Zn(NO₃)₂·6H₂O and Co(NO₃)₂·6H₂O, with designed molar ratios of 25 : 75, 50 : 50, 75 : 25 and 100 : 0, was dissolved in 200 mL of methanol. Then, a solution of 80 mmol 2-methylimidazole dissolved in 200 mL of methanol was added to the flask. The brown mixture was stirred continuously for 12 h at room temperature (25 °C). After centrifugation, the product was washed with methanol several times and dried at 80 °C overnight. Then, these Co/Zn-ZIF precursors were annealed under nitrogen flow for carbonization by thermal treatment at 900 °C, and the samples were denoted as Co₀/NC-900, Co_{0.25}/NC-900, Co_{0.50}/NC-900, Co_{0.75}/NC-900 and Co_{1.00}/NC-900.

State Key Laboratory of Fluorine & Nitrogen Chemical, Xi'an Modern Chemistry Research Institute, Xi'an 710065, China

† Electronic supplementary information (ESI) available. See DOI: <https://doi.org/10.1039/d4ra01816h>





Scheme 1 Synthesis of Co/NC catalysts.

Catalytic tests

The prepared catalyst (10.0 mg) was placed in an oven-dried Schlenk tube evacuated and backfilled with nitrogen (Scheme 2). Solvent 1,2-dichloroethane (2 mL) was added, followed by styrene (2.50 mmol) and a stock solution of ethyl diazoacetate (EDA, 0.5 mmol). The mixture was heated at 60 °C under an N₂ atmosphere; then, the cyclopropanation reaction lasted for 4 h with stirring. After the reaction, the catalyst was separated by centrifugation, and enantiomeric excess and yields were determined by chiral gas chromatography (GC) using an AgilentJ&WDB-35 column on a Shimadzu GC-2014C instrument equipped with an FID detector. The flow rate was set to 3.0 mL min⁻¹ for all tested compounds. The injector was in split mode 100 : 1, the injection volume was 1 μL and the injector temperature was set to 100 °C, while the detector temperature was set to 280 °C. The conditions for separating individual product enantiomers can be found in the compound characterization section.

Catalyst characterisation

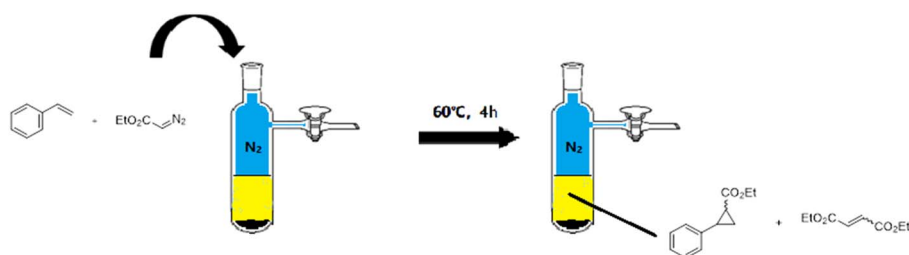
X-ray powder diffractometer (XRD, Rigaku D/Max 2500 VB2 + PC) with 2θ range from 10° to 90° characterized the catalyst powder. Raman spectra were recorded on a LabRAM HR Evolution (Renishaw Invia Raman, UK, 532 nm, 1 cm⁻¹, 100 s). X-ray photoelectron spectroscopy (XPS, Pekin-Elmer PHI-1600) characterized the surface elemental composition and valence using an X-ray source of mono-chromatic Al Kα (1486.6 eV) 150 W (spot size 500 μm). Transmission electron microscopy (TEM, FEI Tecnai-G2F20) characterized the microstructure, combined with Energy Dispersive X-Ray Spectroscopy (EDS) to obtain elemental mapping within the micro-region of the material. The nitrogen adsorption-desorption was performed using a Micromeritics ASAP 2020 at 77 K. Brunauer-Emmett-teller (BET) equiv. was used to calculate the final specific surface area.

Results and discussion

Characterisation of catalysts

The crystal structure investigation of products with different molar ratios of Zn/Co was conducted using powder X-ray diffraction (XRD). Fig. 1a illustrates the results, revealing broad diffraction peaks at 2θ of 25.4° corresponding to the graphitic carbon (002) in all samples.³⁷ Notably, no discernible peaks characteristic of zinc or zinc compounds were evident in the patterns, indicating the effective removal of Zn through evaporation during pyrolysis at 900 °C. By increasing the cobalt content in Zn/Co-ZIF, distinct diffraction peaks associated with metallic Co became evident in the Co/NC samples. Specifically, the peaks at 44.2°, 51.5° and 75.8° were well-indexed to the (111), (200), and (220) planes of fcc-structured metallic Co.³⁸ According to the Scherrer equation, the calculated diameters of metallic Co in Co_{0.25}/NC-900, Co_{0.50}/NC-900, Co_{0.75}/NC-900, and Co_{1.00}/NC-900 were 5.24 nm, 19.6 nm, 21.2 nm, and 27.9 nm, respectively. When the molar ratios of Co content in Co/Zn-ZIF surpassed 50%, there was a significant increase in the size of Co metal particles in the Co/NC materials. This phenomenon was further validated through TEM images, suggesting that a higher cobalt proportion (beyond 50%) triggers the thermal polymerization of metallic cobalt during pyrolysis, ultimately diminishing the catalyst's reaction activity.

The Raman spectra of Co/NC samples are presented in Fig. 1b, revealing the characteristic G band (at 1585 cm⁻¹) associated with graphitic carbon, and the D band (at 1353 cm⁻¹) indicates disordered carbon.³⁹ The relative peak intensity ratio of D to G (*I_D*/*I_G*) serves as a measure of the graphitization degree of carbon materials. The *I_D*/*I_G* ratios for these samples (Co/Zn, 0.25 : 0.75, 0.5 : 0.5, 0.75 : 0.25, 1.0 : 0) are observed to be 1.05, 1.01, 0.95, and 0.87, respectively. This trend suggests that an increase in Co content and a decrease in Zn content result in the generation of more graphitic carbon and fewer defects. This phenomenon may be attributed to the porous structure formed



Scheme 2 Catalytic tests of Co/NC catalysts.

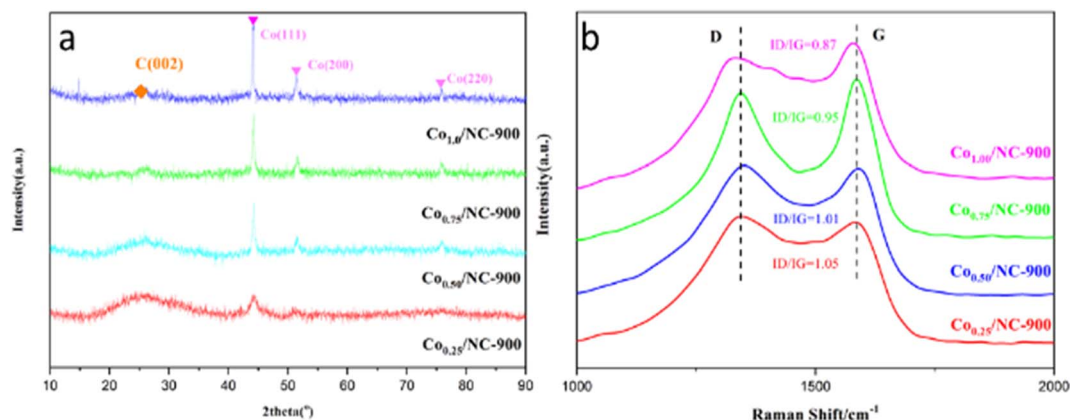


Fig. 1 (a) XRD pattern of Co/NC catalysts and (b) Raman spectra of the Co/NC catalysts.

through the high-temperature evaporation of metallic zinc during the process.⁴⁰

The morphologies and microstructures of the samples were further tested using TEM. The TEM images of Co/NC are shown in Fig. 1a–e. There are no obvious lattice fringes, suggesting the low crystallinity of carbon. Meanwhile, no obvious metal Co NPs were observed in Co₀/NC-900 and Co_{0.25}/NC-900. When the content of Co increases to 50%, several Co metal particles are clearly visible, which agrees with the results of XRD. A high-resolution TEM image of an individual Co NP shows that the Co NP is wrapped by graphitized NC nanosheets (Fig. 2f), which can be reasonably explained by the fact that the sintered Co metal nanoparticles are covered by a graphite layer produced by carbonization. The lattice spacing of the Co_{0.50}/NC-900 was 0.24 nm, which was in accordance with the (111) planes of metallic Co fcc crystals. No lattice fringes ascribed to metal oxide of Co are found, which is in accordance with the result of XRD. Another group of fringes with *d* spacings 0.34 nm matched well with the (002) planes of graphitic carbon.⁴¹

As depicted in Fig. 3, the related elemental maps show the presence of Co, N, and O on the carbon support. The elemental mapping images reveal the homogeneous distribution of Co, C, and N elements, and many microstructures in Fig. 3a with the Co atoms are surrounded by nitrogen atoms, which shows the presence of dispersed Co-N_x clusters at the nitrogen-doped carbonaceous support.

XPS was further applied to explore the composition of surface elements and the chemical states of Co/NC samples. A typical XPS survey of the as-obtained composites demonstrates the presence of C, N, O and Co elements in the samples, as shown in Table 1. The results of Co_{0.75}/NC-900 and Co_{1.00}/NC-900 with N and Co content on the surface were reduced significantly when the Co/Zn ratio increased. However, XRD detection confirms a large diameter cobalt metal, which means that the Co content on the surface becomes metallic cobalt in bulk by thermal polymerization.

As shown in Fig. 4a, an additional peak at 780.8 eV in the Co 2p spectrum was observed, corresponding to Co-N_x. The

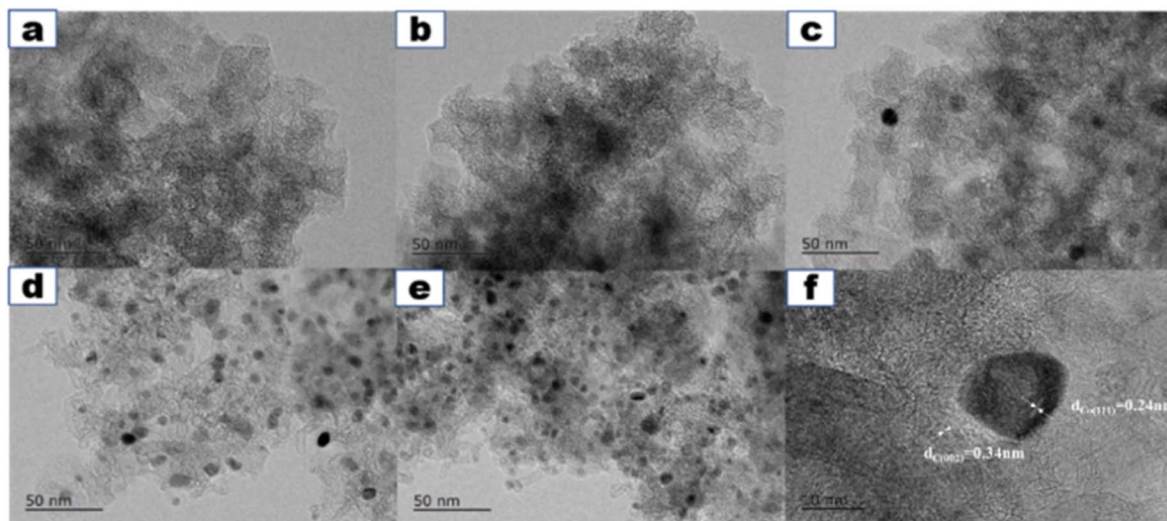


Fig. 2 (a–f) HRTEM images of Co₀/NC-900, Co_{0.25}/NC-900, Co_{0.50}/NC-900, Co_{0.75}/NC-900 and Co_{1.00}/NC-900; (f) particle Co size distributions of Co_{1.00}/NC-900.



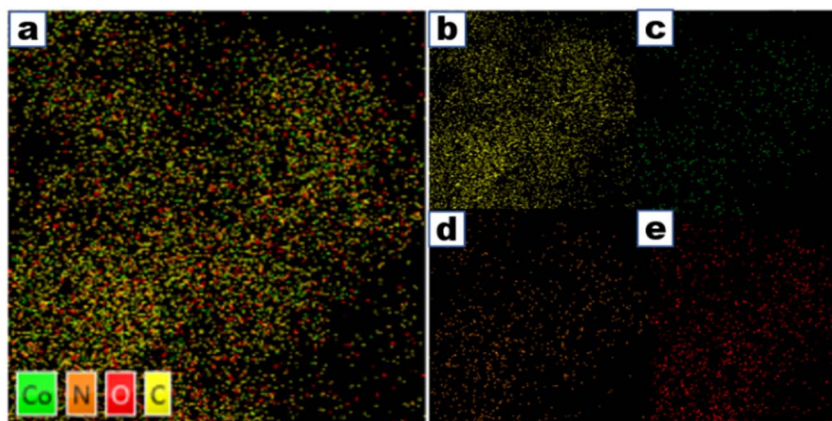


Fig. 3 (a) EDS and elemental mapping of $\text{Co}_{0.50}/\text{NC-900}$, and (b–e) the distribution of the C, Co, N, and O elements.

Table 1 Texture properties of Co/NC catalysts

Catalyst	C [at%]	N [at%]	O [at%]	Co [at%]
$\text{Co}_{0.25}/\text{NC-900}$	81.55	10.77	6.65	0.74
$\text{Co}_{0.25}/\text{NC-900}$	79.72	11.71	7.57	0.94
$\text{Co}_{0.25}/\text{NC-900}$	87.08	7.64	4.81	0.28
$\text{Co}_{0.25}/\text{NC-900}$	95.33	0.20	4.33	0.14

binding energies of samples Co/NC located at 782.3 eV and 799.2 eV correspond to $\text{Co}^{2+} 2\text{p}_{3/2}$ and $\text{Co}^{2+} 2\text{p}_{1/2}$, respectively.⁴² The shake-up satellite peaks at around 5 eV above the main peaks can be further proved by the presence of surface Co^{2+} species, such as Co-O .³⁶ The Co-N_x peak became more dominant and reached the maximum with an increase in the Co/Zn molar ratio to 1 : 1. Then, excessive Co content resulted in

a decrease in the Co-N component. When the Co/Zn molar ratio increased, the peaks situated at the binding energies of 778.3 eV and 793.7 eV were observed, which can be consistent with $\text{Co } 2\text{p}_{3/2}$ and $\text{Co } 2\text{p}_{1/2}$ of metallic Co, respectively.

Fig. 4b illustrates the N 1s XPS spectrum, revealing intriguing details about the composition. An additional peak, discernible at 399.2 eV, is identified as Co-N_x content within the N 1s spectrum, mirroring a similar trend observed in the Co 2p spectrum. Moreover, the N 1s spectra for all samples undergo deconvolution, unveiling distinct peaks at 398.3 eV, 400.8 eV, and 401.6 eV, which correspond to pyridinic N, pyrrolic N, and graphitic N, respectively.⁴³ Notably, the $\text{Co}_{0.50}/\text{NC-900}$ catalyst exhibits the highest percentage of Co-N_x , aligning with its notable activity in the cyclopropanation reaction. Conversely, as the Co content surpasses 50%, there is a noticeable reduction in Co-N_x content. This decline is

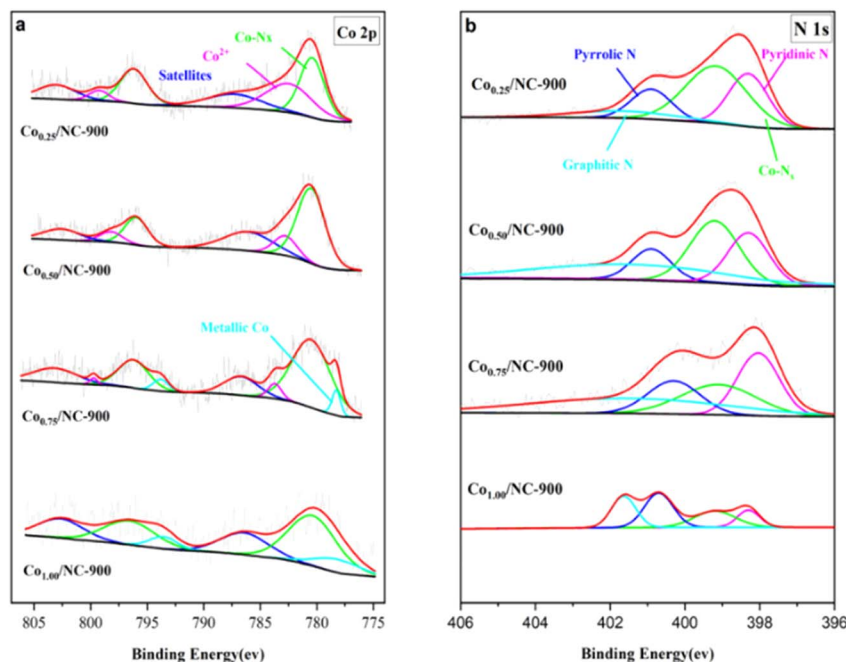


Fig. 4 XPS spectra for the Co/NC catalysts: (a) Co 2p spectrum and (b) N 1s spectrum.

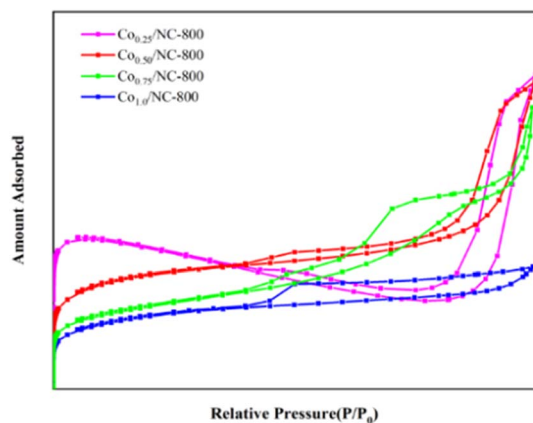


Fig. 5 Nitrogen adsorption-desorption isotherms of Co/NC catalysts.

attributed to the thermal aggregation of cobalt components, leading to the formation of metal particles. Catalysts with lower Co-N_x content demonstrate diminished activity, emphasizing the pivotal role of Co-N_x content as the active site for cyclopropanation Table 3.

The N₂ gas adsorption-desorption isotherm and the corresponding pore size distribution curve of Co/NC-900 are illustrated in Fig. 5. Previous studies show that the ligands can be converted into porous nitrogen-doped carbon materials during the carbonization process, while others decompose into small molecules, such as NH₃ gas; simultaneously, the Co²⁺ and Zn²⁺ ions are reduced *in situ* to metallic Co and Zn NPs.⁴⁰ Then, Zn was removed during pyrolysis at 900 °C by evaporation. The formation of a porous structure is related to the evaporation of Zn at a high temperature, which is beneficial to the transmission of NH₃ molecules and promotes the contact between self-generated NH₃ and tiny amounts of Co particles to form Co-N_x species. As shown in Table 2, when the content of Co is increased by over 50%, less evaporation of Zn content causes a reduction in the pore size and pore volume, and the thermal polymerization of Co metal particles destroys the original high-surface-area zeolite structure of the ZIF precursor, which means that the surface areas of the catalysts decrease significantly.

The above characterization result shows that it is a feasible method to achieve the controllable Co-N_x content in Co/NC by precisely adjusting the molar ratio of the Co/Zn species in the Co/Zn-ZIF precursor. A lower Co/Zn ratio (less than 50%) in Co/Zn-ZIF precursor could inhibit the thermal polymerization of metallic cobalt, then promote the generation of active components (Co-N_x) in Co/NC catalyst, and is also beneficial for improving the porosity and specific surface area of the catalyst.

Table 2 Texture properties of Co/NC catalysts

Catalyst	<i>S</i> _{BET} (m ² g ⁻¹)	<i>V</i> _p (cm ³ g ⁻¹)	<i>d</i> _p (nm)
Co _{0.25} /NC-900	81.55	10.77	6.65
Co _{0.25} /NC-900	79.72	11.71	7.57
Co _{0.25} /NC-900	87.08	7.64	4.81
Co _{0.25} /NC-900	95.33	0.20	4.33

Table 3 Optimization of Co/NC catalysed cyclopropanation of styrene and EDA

Entry	Catalyst	Yield	Selectivity	Trans : cis ratio
1	Co ₀ /NC-900	~ ^a	~	~
2	Co _{0.25} /NC-900	79%	99	75 : 25
3	Co _{0.5} /NC-900	85%	99	77 : 23
4	Co _{0.75} /NC-900	24%	86	68 : 32
5	Co _{1.0} /NC-900	18%	80	72 : 28
6	Co _{0.5} Zn _{0.5} -ZIF	~	~	~
7 ^b	Co _{0.5} /NC-100'	2	23	48 : 52
8 ^b	Co _{0.5} /NC-250'	17	85	69 : 31
9 ^b	Co _{0.5} /NC-550'	33	87	72 : 28
10 ^b	Co _{0.5} /NC-900'	9	84	65 : 35

^a ~ Means no target product was detected. ^b Co/NC catalyst prepared using the impregnation method.

Evaluation of the catalyst for cyclopropanation

The Co/NC catalysts of the cyclopropanation activity of Co/NC catalysts were studied through the cyclopropanation of ethyl diazoacetate (EDA) and styrene. All the experiments were performed at 60 °C with 5 mol% of catalyst in 1,2-dichloroethane, containing 5 equiv. of olefin (2.50 mmol) and 1 equiv. of EDA (0.5 mmol). The activity of Co/NC catalysts was compared in the cyclopropanation of styrene conducted under identical conditions. The results show that the Co-ZIF precursor and Co₀/NC-900 did not have cyclopropanation catalytic activity at all because the yield of the product is 0. The catalytic activity increased with an increased amount of cobalt. The Co_{0.50}/NC-900 catalyst results in the highest yield (85%, Table 1). However, when the ratio of Co is over 50%, the Co-NC catalyst shows a declined activity. This could be related to a decrease in the specific surface area of the Co-NC catalyst and a decrease in the Co-N_x content on the surface.

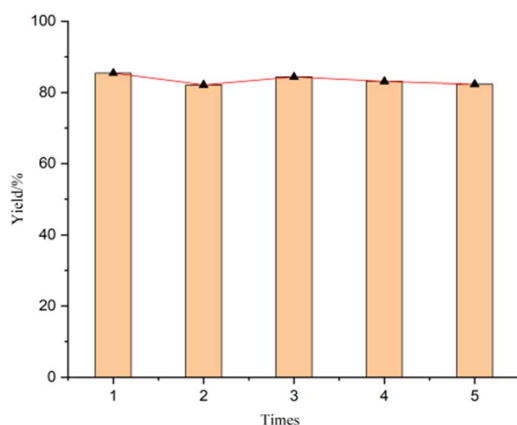
However, when we use the Co/NC catalyst prepared by applying the impregnation method in this reaction, the Co/NC catalyst shows low activity significantly. By treating these Co/NC catalysts at different calcination temperatures, the Co_{0.50}/NC-550 catalyst increases its yield to 33%, though its activity is remains much lower than that of MOF-derived Co/NC catalysts.

Through systematic adjustments in the olefin-to-EDA ratio, we conducted a comparative analysis between MOF-derived Co/NC and Fe/NC catalysts (Table 4). The findings indicate that under conditions where olefins are in excess, the Co-NC catalyst exhibits slightly higher activity than its Fe-NC counterpart, with both demonstrating similar selectivity. However, as the ratio of EDA increases, a substantial decrease in both activity and selectivity is observed for Fe-NC, while the Co-NC catalyst maintains remarkable performance in both aspects. This notable difference is likely attributed to the Co(III)-carbene intermediate state of the catalyst, and a hypothesis is further supported by a detailed comparison of the Co-N_x and Fe-N_x



Table 4 Catalytic performance for the cyclopropanization of Fe and Co catalysts

Entry	Styrene : EDA	Yield	Selectivity	Trans : cis ratio
1 ^a	5 : 1	85%	99%	75 : 25
2 ^a	1 : 1.5	77%	85%	71 : 29
3 ^a	1 : 5	95%	80%	78 : 22
4 ^b	5 : 1	76%	99%	77 : 23
5 ^b	1 : 1.5	45%	78%	75 : 25
6 ^b	1 : 5	68%	61%	61 : 39

^a Co/NC catalyst. ^b Fe catalyst.**Scheme 3** Recycling of Co/NC catalyst for 5 runs.

complexes. The sustained high activity and selectivity of the Co-NC catalyst under varying olefin-to-EDA ratios underscore the significance of the Co(III)-carbene intermediate state in influencing catalytic performance, providing valuable insights into the superior behavior of Co-NC compared to Fe-NC in these experimental conditions.

Stability and recyclability

To demonstrate the practical utility of this catalyst, scalability and recyclability were studied.^{44–46} The model reaction was successfully scaled up to 10-fold without significant variations in activity and selectivity compared to the small-scale run. A slight decrease in the activity was observed after the 5th run (Scheme 3). ICP analysis of the solution showed a negligible (*ca.* 0.1%) loss of cobalt from the catalyst, which means that the Co/NC catalyst is a real heterogeneous catalyst.

Conclusions

In summary, we present the first Co-based heterogeneous catalyst derived from Co/Zn-ZIF by high-temperature pyrolysis. These Co/NC catalysts were characterized and applied in the

cyclopropanation reaction of diazo compounds with a good yield. Furthermore, the catalysts could be easily recovered and reused at least five times without obvious deactivation. Notably, by increasing the Zn content in a molar ratio of Co/Zn of the ZIF precursor, the Co-N_x active sites were effectively regulated, which significantly improved cyclopropanation activity. This simple strategy was developed to regulate active sites, which could contribute to adjusting the activity of catalysts for typical organic reactions with sluggish kinetic processes.

Data availability

All relevant data are within the manuscript and its additional files.

Author contributions

Xin Yue: conceptualization, formal analysis, writing – original. Jiangwei Li: writing – review & editing, Chunying Li: data curation, formal analysis. Zhixuan Wang: visualization, investigation. Yongmei Du: investigation. Daoan Sun: funding acquisition. Hui Ma: investigation. Jian Lu: resources.

Conflicts of interest

There are no conflicts to declare.

Acknowledgements

We thank Specialized National Science Foundation of China (GNTQXL) for financial support.

Notes and references

- 1 J. M. Fraile, B. García, J. I. García, J. A. Mayoral and F. Figueras, *Stud. Surf. Sci. Catal.*, 1997, **108**, 571–578.
- 2 L. A. Wessjohann, W. Brandt and T. Thiemann, *J. Chem. Rev.*, 2003, **103**, 1625–1648.
- 3 C. J. Thibodeaux, W.-c. Chang and H.-w. Liu, *Chem. Rev.*, 2012, **112**, 1681–1709.
- 4 H. E. Simmons and R. D. Smith, *J. Am. Chem. Soc.*, 1959, **81**, 4256–4264.
- 5 H. Nozaki, S. Moriuti, M. Yamabe and R. Noyori, *J. Tetrahedron Lett.*, 1966, **7**, 59–63.
- 6 W. R. Moser, *J. Am. Chem. Soc.*, 1969, **91**, 1135–1140.
- 7 W. v. E. Doering and A. K. Hoffmann, *J. Am. Chem. Soc.*, 1954, **76**, 6162–6165.
- 8 O. G. Kulinkovich, S. V. Sviridov, D. A. Vasilevskii and T. S. Pritytskaya, *Zh. Org. Khim.*, 1989, **25**, 2244–2245.
- 9 G. Bartoli, G. Bencivenni and R. Dalpozzo, *Synthesis*, 2014, **46**, 979–1029.
- 10 S. Inoue, K. Nagatani, H. Tezuka, Y. Hoshino and M. Nakada, *Synlett*, 2017, **28**, 1065–1070.
- 11 M.-I. Picher and B. Plietker, *Org. Lett.*, 2020, **22**, 340–344.
- 12 S.-F. Zhu and Q.-L. Zhou, *Natl. Sci. Rev.*, 2014, **1**, 580–603.



- 13 H. S. A. Mandour, Y. Nakagawa, M. Tone, H. Inoue, N. Otag, I. Fujisawa, S. Chanthamath and S. Iwasa, *Beilstein J. Org. Chem.*, 2019, **15**, 357–363.
- 14 A. DeAngelis, R. Panish and J. M. Fox, *Acc. Chem. Res.*, 2016, **49**, 115–127.
- 15 Y. Wang, X. Wen, X. Cui, L. Wojtas and X. P. Zhang, *J. Am. Chem. Soc.*, 2017, **139**, 1049–1052.
- 16 S. Inoue, K. Nagatani, H. Tezuka, Y. Hoshino and M. Nakada, *Synlett*, 2017, **28**, 1065–1070.
- 17 X. Liu, Y. Liu, X. Li, S. Xiang, Y. Zhang, P. Ying, Z. Wei and C. Li, *Appl. Catal., A*, 2003, **239**, 279–286.
- 18 M. L. Kantam, V. S. Jaya, M. J. Lakshmi, B. R. Reddy, B. M. Choudary and S. K. Bhargava, *Catal. Commun.*, 2007, **8**, 1963–1968.
- 19 S. Ishikawa, R. Hudson, M. Masnadi, M. Bateman, A. Castonguay, N. Braidy, A. Moores and C.-J. Li, *Tetrahedron*, 2015, **71**, 2585.
- 20 L. Chen, M. O. Bovee, B. E. Lemma, K. S. M. Keithley, S. L. Pilson, M. G. Coleman and J. Mack, *Angew. Chem., Int. Ed.*, 2015, **54**, 11084–11087.
- 21 L. R. Chen, D. Leslie, M. G. Coleman and J. Mack, *Chem. Sci.*, 2018, **9**, 4650–4661.
- 22 H. Luo, C. Lin, H. B. Zhou, Y. J. Zhao, X. M. Wang, D. W. Zhang and Y. Yu, *Adv. Mater. Interfaces*, 2022, **9**, 2102110.
- 23 R. L. Safiullin, V. A. Dokichev, L. R. Yakupova, R. M. Sultanova, S. L. Khursan, R. N. Zaripov and Y. V. Tomilov, *Kinet. Catal.*, 2008, **49**, 43–51.
- 24 B. J. Anding, A. Ellern and L. K. Woo, *Organometallics*, 2012, **31**, 3628–3635.
- 25 M. M. Díaz-Requejo, M. C. Nicasio and P. J. Pérez, *Organometallics*, 1998, **17**, 3051–3057.
- 26 J. Rong, E. R. Gao, N. C. Liu, W. Y. Chen, X. S. Rong, Y. Z. Zhang, X. D. Zheng, H. S. Ao, S. L. Xue, B. Huang, Z. Y. Li, F. X. Qiu and Y. T. Qian, *Energy Storage Mater.*, 2023, **56**, 165–173.
- 27 X. Yang, J. Chen, W. Yang, H. Lin and X. Luo, *J. Inorg. Chem. Front.*, 2019, **6**, 3475–3481.
- 28 X. Chen, N. Wang, K. Shen, Y. Xie, Y. Tan and Y. Li, *ACS Appl. Mater. Interfaces*, 2019, **11**, 25976–25985.
- 29 S. Zhou, X. Wang, P. Zhao, J. Zheng, M. Yang, D. Huo and C. Hou, *Microchim. Acta*, 2021, **188**, 383.
- 30 Y. Zhang, J. Y. Wu, S. H. Zhang, N. Z. Shang, X. X. Zhao, S. M. Alshehri, T. Ahamad, Y. Yamauchi, X. T. Xu and Y. Bando, *Nano Energy*, 2022, **97**, 107870.
- 31 Y. T. Zhang, S. Y. Li, N. N. Zhang, G. Lin, R. Q. Wang, M. N. Yang and K. K. Li, *New Carbon Mater.*, 2023, **38**, 200–210.
- 32 Q. Xu, R. Q. Qiu, H. Jiang and X. M. Wang, *J. Electroanal. Chem.*, 2019, **839**, 247–255.
- 33 Y. F. Zhu, D. Y. Zhu, Y. Chen, Q. Q. Yan, *et al.*, Porphyrin-based donor–acceptor cofs as efficient and reusable photocatalysts for pet-raft polymerization under broad spectrum excitation, *Chem. Sci.*, 2021, **12**, 16092–16099.
- 34 Z. Fu, X. Wang, A. M. Gardner, *et al.*, A stable covalent organic framework for photocatalytic carbon dioxide reduction[J]. Royal Society of Chemistry, *Chem. Sci.*, 2020, **11**, 543–550.
- 35 A. Sarkar, D. Formenti, F. Ferretti, C. Kreyenschulte, S. Bartling, K. Junge, M. Beller and F. Ragaini, *Chem. Sci.*, 2020, **11**, 6217–6221.
- 36 H. Zhou, S. Hong, H. Zhang, Y. Chen, H. Xu, X. Wang, Z. Jiang, S. Chen and Y. Liu, *J. Appl. Catal., B*, 2019, **256**, 117767.
- 37 X. Wang, Y. Sun, R. Cai, Z. Jiang, J. Ren, L. Zhang, D. Li, X. Zhao and D. Yang, *J. Alloys Compd.*, 2022, **908**, 164638.
- 38 J. Hu, J. Chen, H. Lin, R. Liu and X. Yang, *J. Solid State Chem.*, 2018, **259**, 1–4.
- 39 O. Maslova, M. Ammar, G. Guimbretière, J.-N. Rouzaud and P. Simon, *Phys. Rev. B: Condens. Matter Mater. Phys.*, 2012, **86**, 134205.
- 40 S. J. Lai, L. Xu, H. L. Liu, S. Chen, R. S. Cai, L. J. Zhang, W. Theis, J. Sun, D. J. Yang and X. L. Zhao, *J. Mater. Chem. A*, 2019, **7**, 21884–21891.
- 41 X. Song, L. Guo, X. Liao, J. Liu, J. Sun and X. Li, *J. Small*, 2017, **13**, 1700238.
- 42 Z. Meng, S. Cai, R. Wang, H. Tang, S. Song and P. Tsiakaras, *J. Appl. Catal., B*, 2019, **244**, 120–127.
- 43 L. Zhang, Z. Su, F. Jiang, L. Yang, J. Qian, Y. Zhou, W. Li and M. Hong, *J. Nanoscale*, 2014, **6**, 6590–6602.
- 44 P. Kate, V. Pandit, V. Jawale and M. Bachute, L-proline catalyzed one-pot three-component synthesis and evaluation for biological activities of tetrahydrobenzo[b]pyran: evaluation by green chemistry metrics, *J. Chem. Sci.*, 2022, **134**(1), 1–11.
- 45 P. Chhattise, S. Saleh, V. Pandit, S. Arbuji and V. Chabukswar, ZnO nanostructures: a heterogeneous catalyst for the synthesis of benzoxanthene and pyranopyrazole scaffolds via a multi-component reaction strategy, *Mater. Adv.*, 2020, **1**, 2339–2345.
- 46 S. S. Pandit, V. U. Pandit and B. P. Bandgar, Rapid and efficient synthesis of sulfonamides from sulfonic acid and amines using cyanuric chloride-dmf adduct, *Sulfur Rep.*, 2008, **29**(6), 619–622.

